Fuel Jet in Cross Flow: Experimental Study of Spray Trajectories at Elevated Pressures and Temperatures

E. Lubarsky*, D. Shcherbik, O. Bibik, J. Bennewitz and B. T. Zinn

School of Aerospace Engineering
Georgia Institute of Technology
Atlanta, Georgia 30332-0150 USA
el45@mail.gatech.edu

N. Patel and M. Benjamin

GE Aviation
General Electric Company
Cincinnati, Ohio 45215 USA

Abstract

This paper describes an experimental investigation of the spray created by Jet-A fuel injection into the cross flow of air at elevated pressures and temperatures. Fuel was injected from a 0.671 mm diam. orifice with flow coefficient of, C_D=0.683. Orifice was incorporated into the wall of a rectangular air channel. Pressure of air in the channel was P~200KPa and temperature was T=590K and 700K, velocity of the flow was V=75m/s. Turbulence level in the core of the flow was about ~2%, thickness of the boundary layer was ~3mm. The momentum flux ratio of the fuel jet to the crossing air was kept in a range between J=5 to J=40. Images of the spray were captured using a high speed camera at a rate of 24,000fps. Exposure time was minimized by using short flashes (30ns) of a copper-vapor laser synchronized with the camera shatter. This methodology allowed obtaining statistically relevant maximum, mean and fluctuating characteristics of spray penetration into the cross-flow. Simple correlations for spray trajectories were obtained using only two empirical coefficients. Spray penetration was found to be proportional to the square root of momentum flux ratio and independent of the Weber (We) number in the investigated range. The spray shape was well determined with the logarithmic function.

Introduction

Cross flow fuel injection is widely used in gas turbine engine combustors, thus it is important to understand the mechanisms that control the breakup of the liquid jet and penetration and distribution of droplets. Such data is needed for validation of CFD codes that will subsequently be incorporated into engine design tools. Additionally, this information is needed for development of qualitative approaches for solving problems such as combustion instabilities [1] and reduction of harmful NOx emissions from aircraft engines. One of the several approaches to solve these problems was by creating a fuel lean homogeneous fuel-air mixture (LPP) just upstream of the combustor inlet. Creating such a mixture requires fine atomization and careful placement of fuel to achieve a high degree of mixing. Liquid jet in cross flow, being able to achieve both these requirements, has gained interest as a likely candidate for spray creation in LPP ducts [2].

Spray penetration into cross flow has received significant attention by experimentalists as preparation and placement of fuel in a modern combustor is crucial for its design. In the 1990s researchers [3] and [4] carried out experiments of jets in air cross flows at different momentum flux ratios using water jets and developed a correlation of the dependence of the jets' upper surface trajectory with liquid to air momentum flux ratio. Later [5] Mie scattering images were used to find the effect of momentum flux ratio, Weber number (We) and liquid viscosity on jet penetration. As in other previous studies, they found that increasing momentum flux ratio increased penetration. Increasing the Weber number decreased the average droplet size and since smaller droplets decelerate faster, the over-

* Corresponding author: el45@mail.gatech.edu

all penetration of the spray decreased. However, many of these correlations are applicable to specific operating conditions, injector geometries and measurement techniques.

In the previous study, [6] the authors measured jet in cross flow spray penetration into a cold air flow. Spray trajectories were found to be independent of Weber number in the investigated range between *We=400* and *We=1600* because only the shear breakup mode of liquid jet disintegration occurs in this range. Spray penetration was found to be proportional to the square root of momentum flux ratio of the fuel jet to crossing air in the range between *J=5* and *J=100*. Simple correlations for the spray trajectories were obtained using only two empirical coefficients. One of them corresponded to the shape of the injector internal path and the other one adjusted the shape of the logarithmic function that determined the average or maximum penetration of the spray and was independent of the injector design.

The main objective of the current study was to develop correlations for spray penetration at elevated temperatures of the crossing air flow. Fuel injector was used in two mounting configurations, 'Spray-well' and 'Flush'.

In order to achieve this goal, a high-temperature test facility was designed and constructed. The methodology for high speed imaging of the spray and processing of the movies for obtaining statistically relevant spray trajectories was developed. "Frozen" images of the spray illuminated with short 30ns flashes of a copper vapor laser were captured at 24,000fps.

Experimental Setup

Figure 1 shows a schematic of the test facility used to study the injection of a liquid jet into the cross flow of air at elevated pressure. This setup had a plenum chamber, a rectangular air supply channel, a test section with injector under investigation and a pressurized chamber with four 38mm thick windows for optical access to the spray.

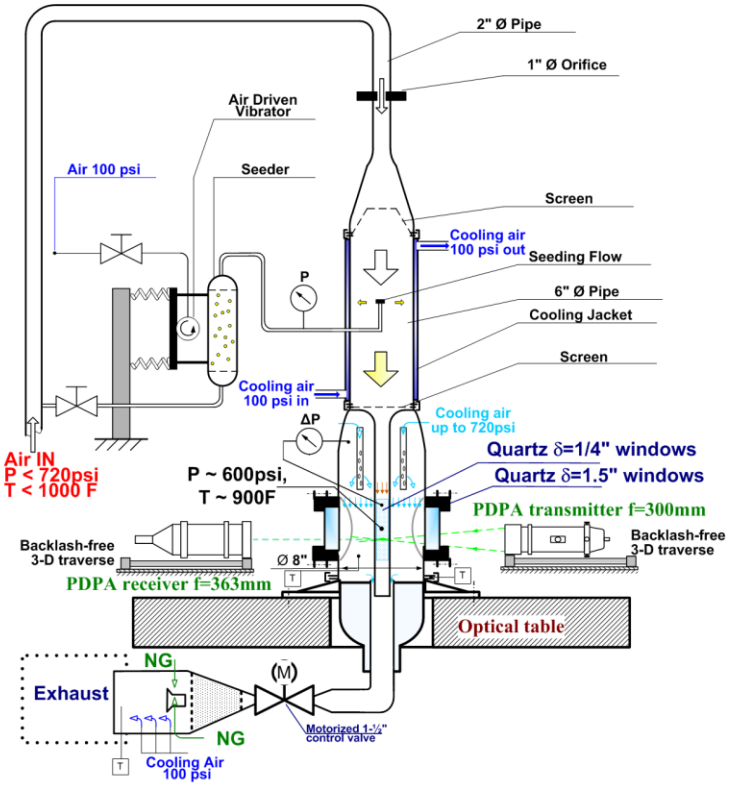

Figure 1 Schematic of the test facility.

Plenum chamber was 203.2 mm in diam. and 457.2mm long. The rectangular supply channel was 62.3mm × 43.2mm in cross-section and was 304.8mm long. It was equipped with a "bell-mouth" which was connected to the bottom of the plenum chamber to smoothen the air flow. On the other end of the channel four aerodynamically shaped plates were attached to the channel creating a test section with a cross-section 31.75×25.4mm.

This test section has ~50mm long with 6mm thick windows on three sides. Fourth side was used for injector installation.

Velocity in the test section was controlled by the valve in the exhaust line. Cooling of the test channel and test section was achieved by purging the pressure vessel with the high pressure air flow (P<5.0MPa, T~295K). Pressure of this cooling air was slightly higher than in the test section to keep temperature in it's surrounding below T=100^{0}C. Mixture of this cooling air, process air passing the test section and injected fuel left rig through the exhaust line, control valve, and scavenging afterburner where this fuel to air mixture was burned in the pilot flame of natural gas to prevent fuel from entering the atmosphere.

Flow conditions in the test section were monitored using a Pitot tube and thermocouple, which were located within the test channel (see Figure 2-a). Axes of the coordinate system used in this study were designated as shown on the Figure 2-b.

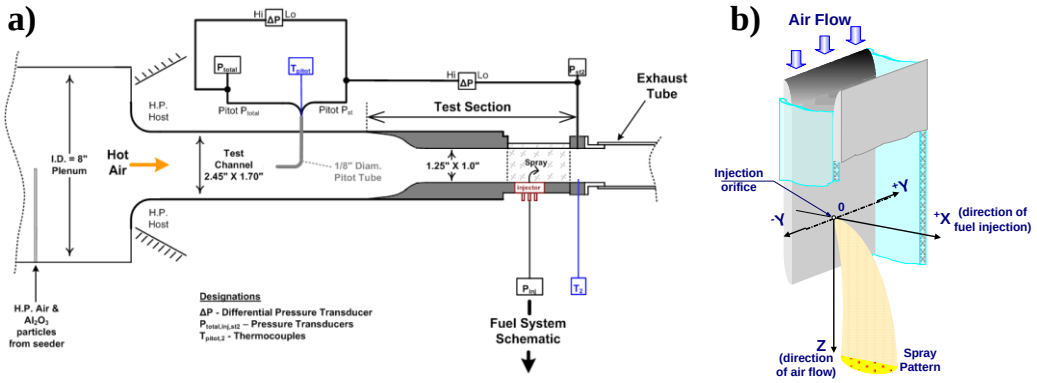

Figure 2 Instrumentation of the test section (a) and coordinate system for spray characterization (b).

Characterization of the flow in the test section was performed using three dimensional (3-D) Laser Doppler Velocimeter (LDV). This LDV consisted of two transceivers oriented 90 degrees apart, was installed on the 3-D traversing mechanism for scanning through the test section upstream and downstream of the injector to measure velocity profile. Incoming flow was seeded with 3-5 micron Al_2O_3 particles through the seeding port in the plenum section (see Figure 1). The incoming velocity profile (see Figure 3) for the test section was found to be uniform, with the boundary layer thickness ~ 3 mm. and the level of turbulence in the free stream flow about 2%.

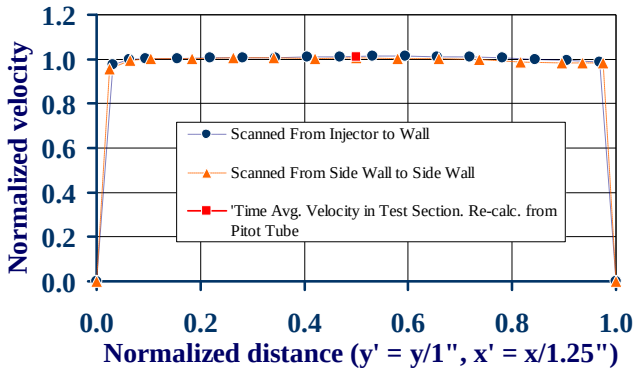

Figure 3 Axial velocity profiles measured in a cross section 5 mm upstream of the injection orifice

Jet-A aviation fuel was supplied to the injector installed in the test section through the line equipped with filters, remotely controlled fuel metering unit and turbine flow meters. Fuel temperature was monitored by the thermocouple installed in the supply line. Fuel pressure transducer was connected to the special "instrumentation" port on the injector. Rig was also equipped with the return (bypass) line which allowed certain part of the supplied fuel pass through the injector back to the tank. A fuel purge system which uses high pressure N_2 (optimized for ΔP ~ 100 psi across the injector) has been implemented to avoid cooking of the fuel after cut offs, while the test channel and injector are exposed to hot air during test runs.

The fuel injector had internal diameter I.D=0.671mm. It was able to be mounted using adaptors, either 'Spraywell' or 'Flush'. As the name suggests, the 'Flush' mount permits the spray to be injected flush from the test section wall, while the 'Spraywell' mount causes the spray to be injected in a cavity as shown on the Figure 4.

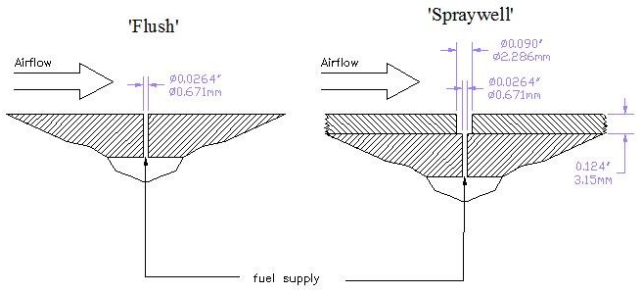

Figure 4 Schematics of the injector mount. 'Flush' (Left) & 'Spraywell' (Right)

Discharge coefficient of the injector was equal to C_d = 0.683. Dependence of the flow coefficient upon varying *Re* numbers (see Figure 5) shows that the discharge coefficient is practically constant over the entire range tested.

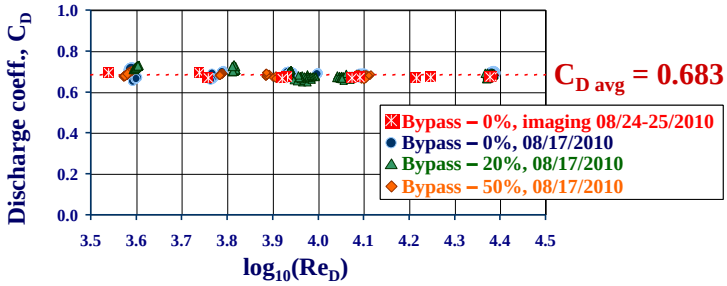

Figure 5 Dependence of the discharge coefficient upon the *Re* number (fuel viscosity was taken 0.001266 Pa-s).

Finally, high-resolution, "macro" and "micro" videos of the fuel jet injected from this injector (with no cross flow of air) were taken. Illumination of the jet was performed by the 30ns laser pulses synchronized with the camera expositions. Examples of the images are shown on the Figure 6.

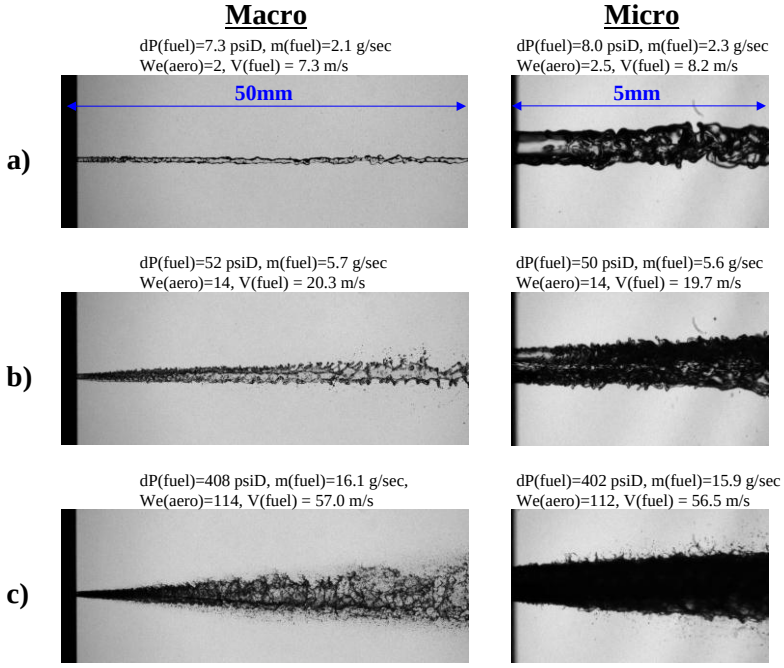

Figure 6 Typical macro- and micro-images of the fuel jet injected from the injector into the atmosphere (no cross flow) at the pressure drops over the injector dP ~ 10 psid (a), 50 psid (b) and 400 psid (c).

Spray imaging and processing

Methodology for the measuring spray trajectories used in this study was based on obtaining statistically relevant series of images, in which an individual image represents an instantaneous ("frozen") picture of spray and each spray movement was represented with not less than 5-10 images. For this purpose high speed shadowgraph imaging technique with short exposition time was chosen. Technically this approach was realized using high speed camera at the rate of 24,000 fps with a record length of ~ 8000 frames. Illumination of the spray was achieved by the copper-vapor laser flashes (30 ns) synchronized with the frame capturing.

High speed camera was positioned directly against the light source provided by the copper-vapor laser to capture the illuminated spray. Laser light was introduced into the test cell through the 1mm diam. quartz fiber. Collimator lens and diffusing glass plate created uniform light beam that illuminated spray from one side through the window in the pressure vessel. Camera that was installed on the other side of the pressure vessel captured shadowgraph images of the spray.

This installation provided opportunity for capturing of high resolution images. An example of the pixel scale for both the general (192×432 pixel=23×50 mm) and near view (308×304 pp=10.7×10.6 mm) images is shown in Figure 7-a and –b respectively.

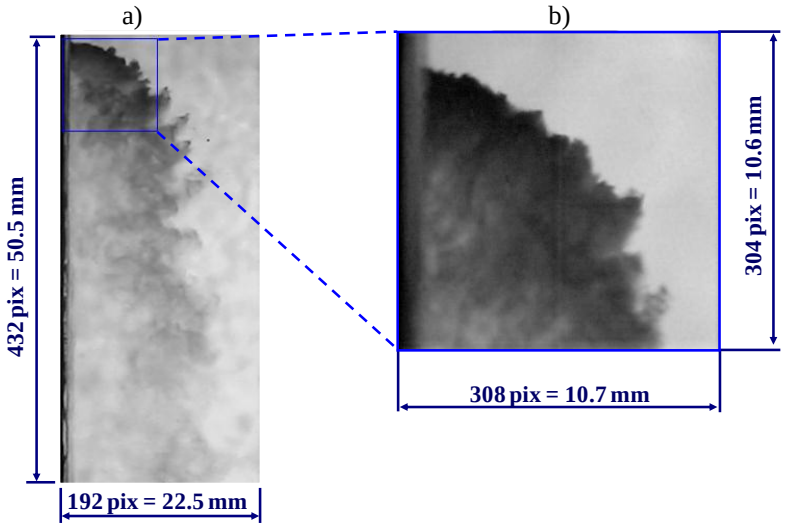

Figure 7 Pixel scales for the general and near view images taken by the high speed camera
a) general view image; b) near view image;

Each of several thousands images that compose a high speed movie of the fluctuating spray was processed individually pursuing a goal of getting outer border of the spray pattern. For this purpose the following procedure was applied:

- Each image was corrected by subtraction of the averaged background. Images of the background were captured before any fuel was injected
- Dynamic range of each image was adjusted to eliminate possible influence of laser pulse intensity fluctuations (i.e. to avoid effect of the overall brightness of the image).
- Threshold was applied to all images in the series to equalize pixel intensity value in the spray region to 'white' and background region pixels to 'black'. Line that divided white and black zones on the image represented outer border of the spray.

Since the result of the spray pattern characterization can be affected by the threshold selection, an analysis was performed to determine the acceptable range of lower threshold values. To generate this range, the mean spray trajectory of a single test was processed using eight different lower thresholds varying from ~ 20% - 63%. A plot comparing these mean spray trajectories for each threshold can be seen in Figure 8 - A. Aside from this plot, Figure 8 includes two additional plots (labeled B & C) comparing the spray trajectory values for each threshold in two regions downstream the injection orifice: z = 0.25 mm (z/d ~ 0.4) and z = 13 mm (z/d ~ 19). From these plots, it can be seen that the acceptable lower threshold ranges from 30% - 50%, because the difference between the spray trajectory values are minimized for the thresholds within this range.

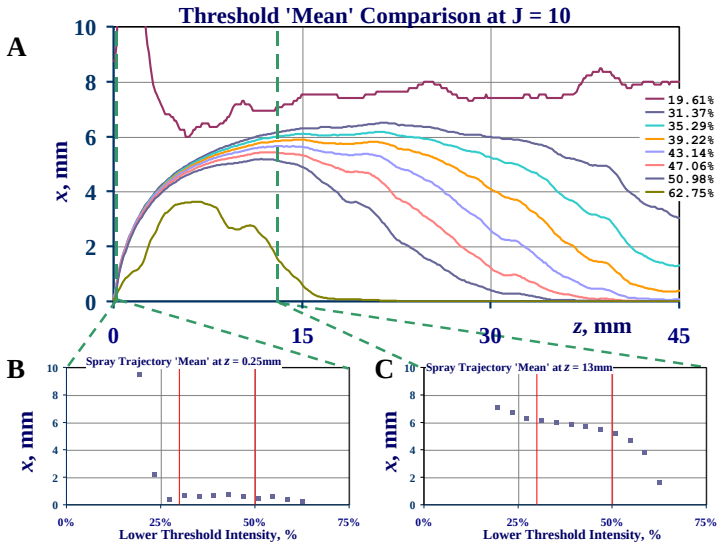

Figure 8 Mean spray trajectory threshold analysis; A) Outer border of the spray at different thresholds; B) and C) Variation of outer border position, *X* vs. lower threshold intensity at downstream distances from the orifice, *Z*=0.25mm and 13mm respectively.

With the 'background correction' and lower pixel intensity threshold applied, the spray trajectory of each image was generated. From this set of trajectories, the mean spray trajectory, '*RMS*' data and maximum spray penetrations were determined over the movie duration.

Results & Discussion

General and near-view images of the spray were captured at the incoming flow temperature of T_{air}=590K, and *T*=700K at air pressure of P_{air}~200KPa for the fuel to air momentum flux ratio's of *J* = 5, 10, 20 and 40.

Spray data comparing the T_{air}=590K (600ºF) and T_{air}=700K (800ºF) test series for momentum ratio *J* ~ 20 with the injector 'Spraywell' mounting were chosen for the analysis. An individual raw images of the spray (background was not subtracted) obtained at two flow conditions to be compared are shown on the Figure 9

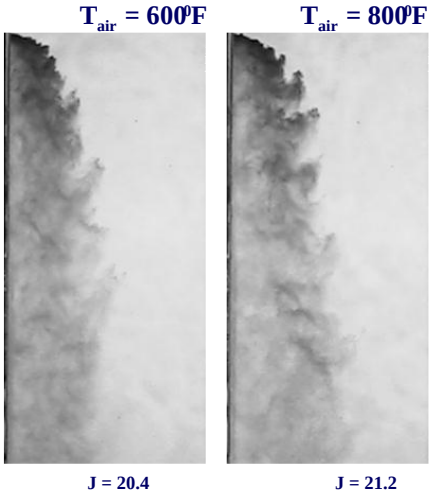

Figure 9. Raw spray images captured at temperatures, *T*=590K (600ºF) and at *T*=700K (800ºF). Momentum flux ratio, *J*~20.

Experimental data obtained in course of spray imaging were used for development of correlation functions that described the spray outer border as a function of longitudinal position downstream from the injection orifice [e.g. *x/d=f(z/d)*]. Literature sources suggest such correlations in several different forms shown in the Table 1 that definite-

ly include power function of the momentum flux ratio J^n. Correlations may or may not include power function of Weber number. Shape of the spray pattern is typically described using logarithmic or power function. In spite of the fact that the accuracy of correlation can be improved by increasing number of empiric constants (from 2 to 8 in the table 1), current study seeks to find an accurate model to fit both the mean spray trajectories and maximum spray penetrations, with the smallest number of regression coefficients possible (target: 2 – 4 coefficients).

Table 1: Various Spray Trajectory Correlation Functions

Model	Function
1	$\frac{x}{d}=A_1\sqrt{J}\ln\left(1+A_2\left(\frac{z}{d}\right)\right)$
2	$\frac{x}{d}=A_1 J^{A_2}\ln\left(1+A_3\left(\frac{z}{d}\right)\right)$
3	$\frac{x}{d}=A_1 J^{A_2} We^{A_3}\ln\left(1+A_4\left(\frac{z}{d}\right)\right)$
4	$\frac{x}{d}=A_1\sqrt{J}\left(\frac{z}{d}\right)^{A_2}$
5	$\frac{x}{d}=A_1 J^{A_2}\left(\frac{z}{d}\right)^{A_3}$
6	$\frac{x}{d}=A_1 J^{A_2} We^{A_3}\left(\frac{z}{d}\right)^{A_4}$
7	$\frac{x}{d}=A_6\sqrt{J}\left(1-e^{-A_1(z/d)}\right)\left(1-A_2e^{-A_3(z/d)}\right)\left(1-A_4e^{-A_5(z/d)}\right)$
8	$\frac{x}{d}=A_6 J^{A_7}\left(1-e^{-A_1(z/d)}\right)\left(1-A_2e^{-A_3(z/d)}\right)\left(1-A_4e^{-A_5(z/d)}\right)$
9	$\frac{x}{d}=A_6 J^{A_7} We^{A_8}\left(1-e^{-A_1(z/d)}\right)\left(1-A_2e^{-A_3(z/d)}\right)\left(1-A_4e^{-A_5(z/d)}\right)$

This was achieved by using self explained proportionality of droplets penetration into the cross flow to their velocity at the point of discharge (i.e. $x/d \sim U_{fuel} \sim J^{0.5}$) and thus reducing number of the empiric constants by one (i,e $J^n = J^{0.5}$). This significant simplification was proved experimentally in the previous study [6] in a wide range of momentum ratios between $J=5$ and $J=100$.

Another simplification was attained by limitation of the Weber number range between We=400 and We=800. This in turn limited number of possible mechanisms of the jet disintegration to only shear breakup excluding column break up. Independence of spray penetration upon the Weber number in the investigated range allowed exclude Weber number from correlations. Based on previous studies [6], the first three models were analyzed and compared to find the most acceptable fit. Finalized model regression coefficient sets were selected by comparing the R^2 value for each tested combination of temperatures and injector mounts. A summary of the optimized regression coefficient sets for Model 1 with corresponding R^2 values (for the provided z/d range) can be seen in the Table 2.

Table 2: Mean/Max spray trajectory regression coefficients summary (Pressure, P=200KPa, Range of momentum ratios, J=5….40, We=400-800) – Model 1

$$\frac{x}{d}=A_{1,mean/Max}\sqrt{J}\ln\left[1+A_{2,mean/Max}\left(\frac{z}{d}\right)\right]$$

Test conditions		A_1		A_2		R_2		z/d
Inj. mount	Tair, K	mean	Max.	mean	Max.	mean	max	range
'Spraywell'	590	0.8287	0.9311	1.4067	2.3840	0.9873	0.9875	0≤z/d≤15
	700	0.8030	0.8741	1.3487	2.5092	0.9869	0.9619	

In fact all R^2 values exceed 98.5% for the mean spray trajectory data, while the R^2 values for the max spray data exceed 90% for the tests in their given z/d range.

Upon comparing the R^2 values for the Model 1 fits of the mean and maximum spray trajectories, for the most part, all of the R^2 values for the maximum spray penetration models are lower than for their mean spray model coun-

terpart. This decrease in goodness of fit can be attributed to fluctuations present in the max spray trajectory test data (making it more difficult for the model to accurately describe the maximum spray trajectory).

Each 'Spraywell' test model was set to cover up to z/d = 15, corresponding to the location where estimated evaporation occurs for the 'Spraywell' tests under high temperature cross flow conditions (i.e. conditions for quickest evaporation). It is in this region where the mean spray trajectory will cease to increase for increasing z/d, hence leading to a deviation between the model and test data. For the 'Flush' injector mounting test however, the model data and the spray trajectory do not begin to deviate until further downstream (z/d = 25).

The same analysis mentioned above was performed for Models 2 & 3 to see if a significant increase in model accuracy would be able to be achieved. By comparing the R^2 values for each model regression combination across the three models, it was found that there is not a large enough improvement in model accuracy for either Model 2 or 3 to be implemented.

Concluding Remarks

1) Outer borders of the Jet-A spray in the cross flow of preheated air at elevated pressure in the 25mm×30mm rectangular test channel were measured by application the high speed imaging technique that allowed obtaining series of instantaneous ('frozen') images of the fluctuating spray.
2) Injector had internal diameter of the orifice I.D=0.671mm and flow coefficient C_D=0.683. Two mounting configurations of the injector were used: 'Spraywell', which created a cavity between the orifice and the wall and 'Flush' when orifice opening was in plane with the channel wall. Crossing air flow had core turbulence ~2% and thickness of the boundary layer near the rectangular channel walls ~3mm.
3) Shadowgraph spray images were captured using high speed camera at a rate of 24,000fps. Length of the record was typically 8000 frames. Exposure time was minimized by using short flashes (30ns) of the copper-vapor laser synchronized with the frame capture.
4) Experimental data obtained in course of spray imaging were used for development of correlation functions that described the spray outer border as a function of longitudinal position downstream from the injection orifice. Simple correlations were obtained using only two empirical coefficients Spray penetration was found to be proportional to the square root of momentum flux ratio and independent upon the Weber number in the investigated range of *We*=400-800. Shape of the spray was well determined with the logarithmic function.
5) More sophisticated correlations with up to four empirical constants were attempted. These included use of momentum flux ratio in power that differs from ½, dependence of penetration upon the *We* number and use of power function instead of logarithmic function to determine spray trajectory. All these attempts did not improve correlations significantly.

Acknowledgements

This research was funded by GE Aviation (General Electric Company) Cincinnati, Ohio 45215 USA with contract monitor Dr. Nayan Patel.

References:

1. Bonnell, J. M., Marchall, R. L., and Riecke, G. T., "Combustion Instability in turbojet and Turbofan Augmentors", AIAA 71-698, *7th AIAA/SAE Propulsion Joint Specialist Conference Exhibi*t, Salt Lake City, UT 1971.
2. Becker, J. & Hassa, C. (2002). Breakup and Atomization of a Kerosene Jet in Cross flow at Elevated Pressure. *Atomization and Sprays*, Vol. 11, pp. 49-67
3. Chen, T. H., Smith, C. R., and Schommer, D. G., "Multi-Zone Behavior of Transverse Liquid Jet in High-Speed Flow," *AIAA Paper*, 93-0453, 1993
4. Wu, P.-K., Kirkendall, K. A., Fuller, R. P., and Nejad, A. S., "Breakup Processes of Liquid Jets in Subsonic Cross-flows," *Journal of Propulsion and Power*, Vol. 13, No. 1, 1997, pp. 64,73.
5. Stenzler, J. N., Lee, J. G., and Santavicca, D. A., "Penetration of Liquid Jets in a Crossflow", AIAA 2003-1327, *41st Aerospace Science Meeting & Exhibi*t, **,** Reno, NV 2003.
6. E. Lubarsky, D. Shcherbik, O. Bibik, Y. Gopala, J. W. Bennewitz, and B. T. Zinn. "Fuel Jet in Cross Flow. Experimental Study of Spray Characteristics" *ILASS Americas, 23rd Annual Conference on Liquid Atomization and Spray Systems, Ventura, CA, May 2011*